ADVANCED FUNCTIONAL MATERIALS

Supporting Information

for *Adv. Funct. Mater.*, DOI: 10.1002/adfm.202005319

Magneto-Mechanical Metamaterials with Widely Tunable Mechanical Properties and Acoustic Bandgaps

S. Macrae Montgomery, Shuai Wu, Xiao Kuang, Connor D. Armstrong, Cole Zemelka, Qiji Ze, Rundong Zhang, Ruike Zhao, and H. Jerry Qi**

WILEY-VCH

Supporting Information

Magneto-Mechanical Metamaterials with Widely Tunable Mechanical Properties and Acoustic Bandgaps

S. Macrae Montgomery[a§], Shuai Wu[b§], Xiao Kuang[a], Connor D. Armstrong[a], Cole Zemelka[b], Qiji Ze[b], Rundong Zhang[b], Ruike Zhao[b]*, H. Jerry Qi[a]*

[a]The George W. Woodruff School of Mechanical Engineering, Georgia Institute of Technology, Atlanta, GA 30332, USA

[b]Department of Mechanical and Aerospace Engineering, The Ohio State University, Columbus, OH, 43210, USA

§ These authors made equal contributions to this work.

*Corresponding authors. Email: zhao.2885@osu.edu; qih@me.gatech.edu;

S1. Unit cell and metamaterial array fabrication

The sample fabrication procedure is depicted in **Figure S1**. The unit cells are fabricated by injecting the magnetic PDMS or the M-SMP precursors into polyvinyl alcohol (PVA) molds 3D printed by using a Creality Ender 5 FDM printer (Creality, Shenzhen, China). Figure S1a shows the printed mold (left) and the unit cell after it is removed from the mold after curing (right). In order to properly align all the unit cells to create the array structure, a fixture was printed on a Connex Objet260 (Stratasys, Eden Prairie, MN, USA). The unit cells are placed in the fixture, as shown in Figure S1b, and special cavities help align the guide tubes for the nylon lines. Additionally, standalone unit cell walls are required to connect unit cells around the edge of the array.

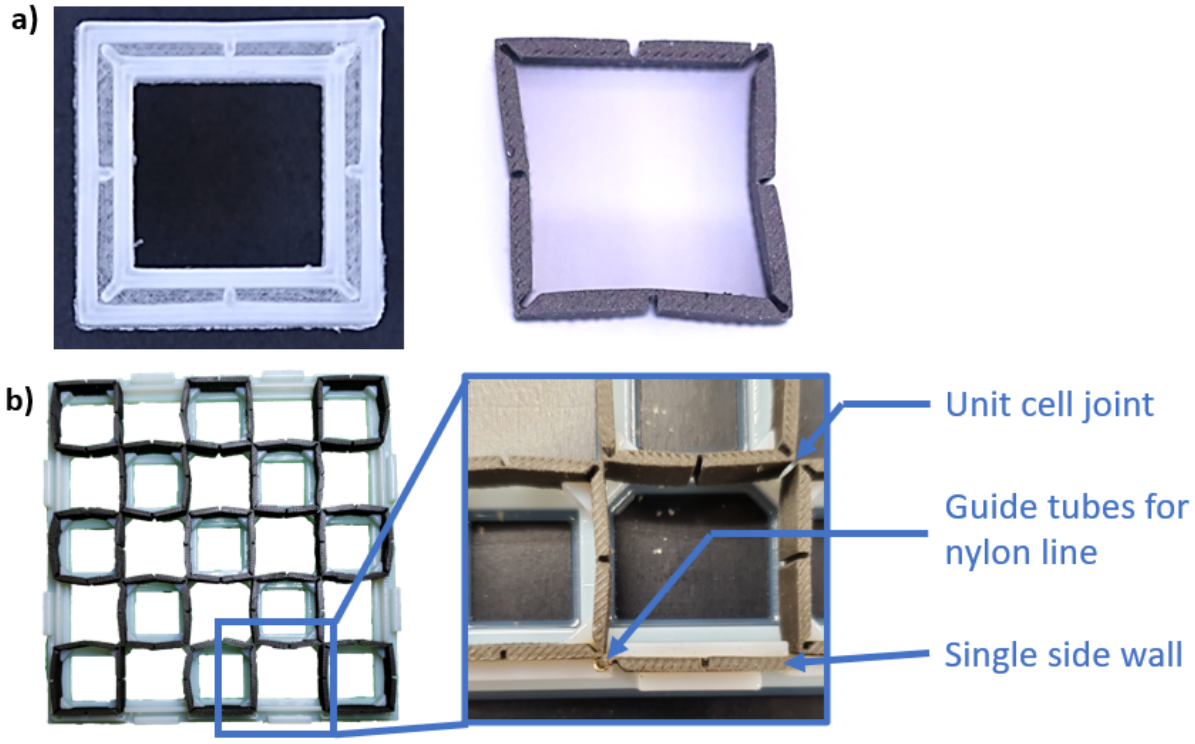

Figure S1. Depiction of the fabrication procedure for unit cells and metamaterial arrays. a) 3D-printed mold before filling with the hmSAM (left) and the as-fabricated unit cell (right). b) Unit cells are arranged on a fixture for proper alignment prior to being fused together. There are additional guiding features to ensure proper placement of the tubes to guide the nylon compression lines and the standalone unit cell walls that connect the cells around the edges of the array.

S2. Unit cell geometry

The precise shape and dimensions of the unit cell used in this work are depicted in **Figure S2**. The chamfers around the openings of the asymmetric joints were designed to account for the resolution limitations of the 3D-printed molds. Figure S2a provides the full view of the unit cell, and Figure S2b depicts the dimensions of the corner and asymmetric joints.

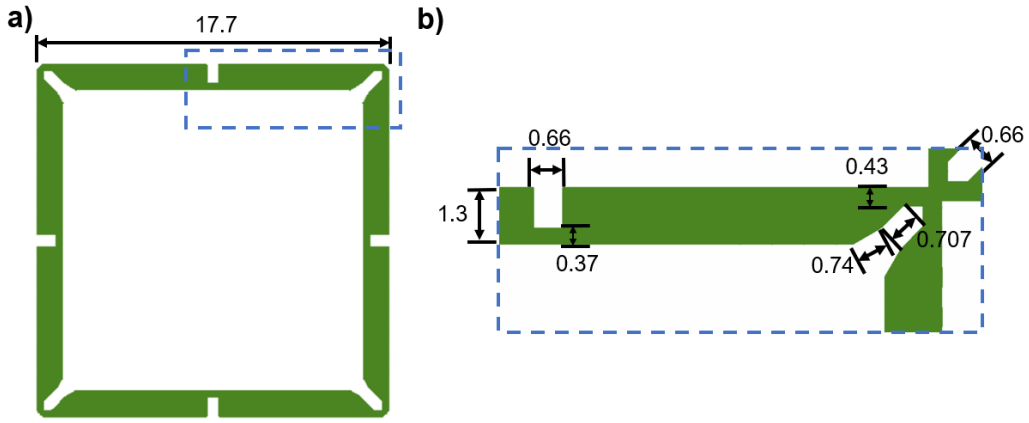

Figure S2. Schematic of the unit cell geometry used for magneto-mechanical metamaterials. a) Front view of the unit cell. b) Enlarged view of the asymmetric joint region. All dimensions are in millimeters.

S3. Experimental test setup

The experimental setup is depicted in **Figure S3**a. The coils were home-made by winding a coated copper wire. A power supply (Preen ADG-L-160-25 DC, AC Power Corp., Taiwan, China) was used to provide the current to generate the magnetic field. The magnetic field was measured at the midpoint along the axis of the two coils. The strength of the magnetic field was close to being constant at the center but increased near the either coil. A camera (Canon EOS Rebel T6i with a 28-135mm lens) was placed above the Helmholtz coils to capture the images and videos during the actuation and mechanical compression. During actuation, the unit cell or the array rested on a piece of Teflon that was sprinkled with 50-70μm particles of sand (Sigma Aldrich, St. Louis, MO, USA) to decrease friction. The samples were connected via 250um nylon lines to a universal material testing machine (Model 41, MTS, Eden Prairie, MN, USA). Lines connected to the left side of the metamaterial were pulled through the center of the right coil and *vice versa* as depicted in Figure S3b. An image of the whole setup is shown in Figure S3c.

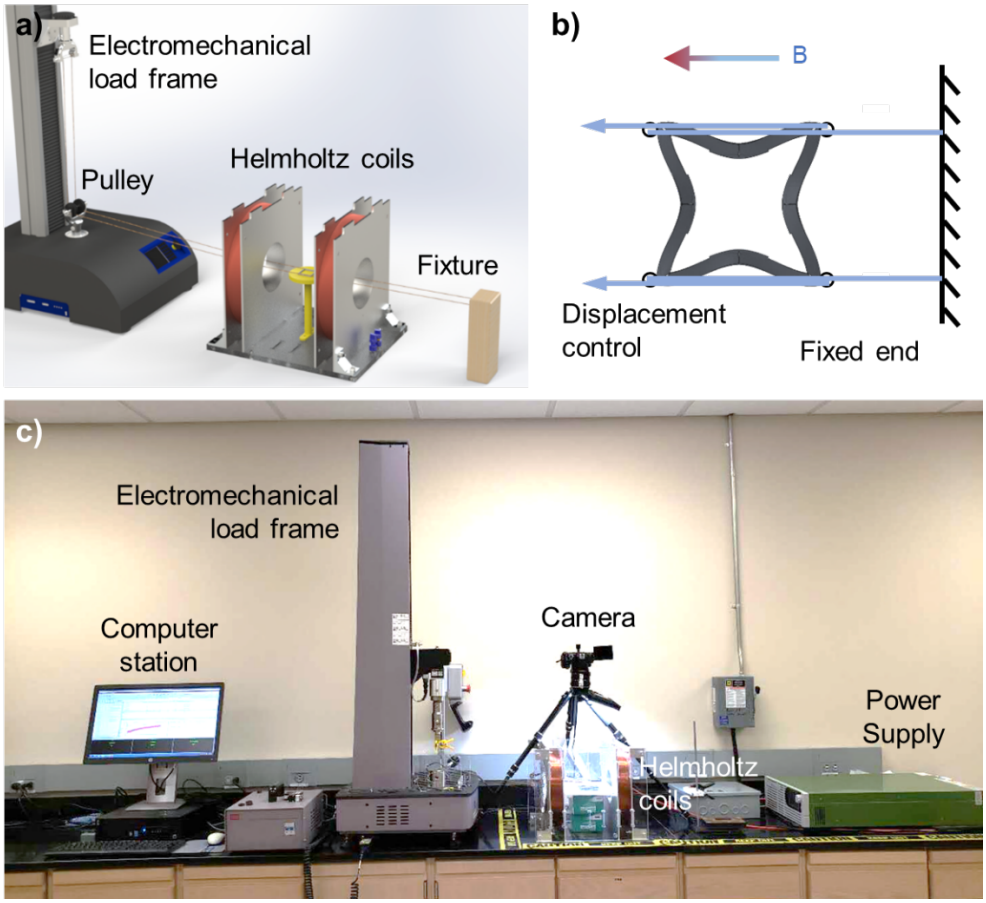

Figure S3. Experimental setup for magneto-mechanical tests. a) The schematics of the experimental setup. b) The schematic of the setup for unit cell loading. c) The photo of the experimental setup.

S4. Finite element analysis simulations

S4.1 Magnetic actuation

Magnetic actuation was predicted using the commercial finite element analysis (FEA) software ABAQUS 2019 package (Dassault Systèmes, Providence, RI, USA). The 8-node user-defined elements for magnetic-responsive materials were utilized for the simulations (1). Magnetization, shear modulus, and bulk modulus for the material were assigned to be 80 $kA \cdot m^{-1}$, 300 kPa, and 30 MPa, respectively. The cells were modeled according to the dimensions of the experimental specimens (See Figure S2). All regions of the cells were assigned the material properties above, with variations occurring only in the magnetization direction to achieve the desired actuation modes. Surface to surface contact was used with the friction coefficient set to be 1. Arrays constructed from the repeating unit cells were created by merging the chamfered corners of the cells to form an assembly.

S4.2 Compression simulations

Deformations during the compression of the magnetically actuated cells or arrays were simulated using ABAQUS. The simulations were conducted using the same models and analysis procedures developed for the magnetic actuation. After ramping up the magnetic field, displacement-controlled loading was applied to compress the cells or arrays while maintaining a constant magnetic field. The displacement-control was assigned to nodes that represented the locations of the pins used in the experiments. The total compression force during compression was extracted. The strains in the x and y direction were defined as $(L\text{-}l_x)/L$ and $(L\text{-}l_y)/L$, respectively, where L was the length of array after magnetic actuation, l_x and l_y were deformed array dimensions in the x and y directions after compression. The Poisson's ratio was defined as the negative ratio between strains in the y and x directions.

S4.3 Acoustic simulations

Phononic bandgap properties of the metamaterial were analyzed using two separate techniques: Bloch wave analysis and dynamic analysis. Both simulations were conducted using ABAQUS. The dynamic analysis used the ABAQUS standard procedure whereas the Bloch wave analysis utilized the frequency extraction procedure described by Åberg & Gudmundson (2). The two analyses are described below.

The Bloch analysis is used to extract the eigenvalues (frequencies) of a periodic structure comprised of infinitely repeated units (or representative volume elements (RVEs)). This approach only involves a single RVE with frequency-dependent periodic boundary conditions applied to the edges simulated under Bloch waves of the form:

$$U(\mathbf{r}) = U_r e^{-i(\omega t - \mathbf{k}\cdot\mathbf{r})}$$

where **k** is the wave vector describing the direction of the wave propagation and **r** is the vector from one point to its corresponding periodic point. It has been asserted by Kittel (3) that all the Bloch waves that can propagate through a structure can be well approximated by analyzing only the wave vectors that define the boundary of the smallest region of symmetry in the RVE. This region is known as the irreducible Brillouin zone (IBZ) (4). Therefore, frequency ranges that do not have a mode in the IBZ represent the bandgaps within which no propagation should occur. This phenomenon is depicted in **Figure S4**a. For the magnetically actuated RVE, due to the four-fold symmetry, the IBZ is a triangle that makes up half of one quadrant of the RVE. Under the mechanical loading, however, the four-fold symmetry becomes two-fold. The new IBZ becomes the full quadrant of the RVE. In this case, the full quadrant, defined by the points Γ, X, M, and Y, cannot be reduced by further symmetry. The IBZs for the RVE are depicted in Figure S4b.

By running the frequency extraction procedure across all the wave vectors around the boundary of the IBZ, a plot of frequencies (or eigenvalues; describing the deformation modes of the unit cell) versus wave vector can be created. Then, by connecting the frequencies of the modes at each wave vector, a plot can be created that depicts how the modes of the structure change with different forcing waves. Any frequency

range through which no modal lines pass is considered to not allow any wave propagation, so these frequency ranges are known as bandgaps.

A dynamic analysis was conducted to confirm the accuracy of the Bloch analysis procedure. In this method, a larger collection of RVEs is driven by a harmonic point force across a range of frequencies. The amplitude of the vibration of a listener node on the opposite side of the model is analyzed. The amplitude of motion of the listener node is expected to drop drastically when the forcing frequency lies within one of the bandgaps discovered from the Bloch analysis. Comparisons of the results from the Bloch analysis and the dynamic analysis for select deformations are shown in Figure S4c-d.

The numerical analysis methods described above are both linear perturbation procedures where non-linear effects cannot be considered. These effects are manifested in the form of material properties, applied magnetic field, and contact. For simplicity, the material properties are treated as linear isotropic, which is a valid assumption for the small strains encountered in a linear perturbation procedure. The motion of the metamaterial within the applied magnetic field may also alter the results due to the complex electromagnetic interaction of the embedded magnetic particles with the field. But this has been shown to be a relatively small effect at the low magnetic fields used here(5, 6). Therefore, this effect was neglected in this work. Contact, on the other hand, is significant in some of the deformation modes achieved by our RVEs. However, since the linear perturbation simulations cannot account for contact (which is a form nonlinearity), we tied the nodes (by using constraints in ABAQUS) when two points are in contact. The tie constraints were maintained during the Bloch wave analysis.

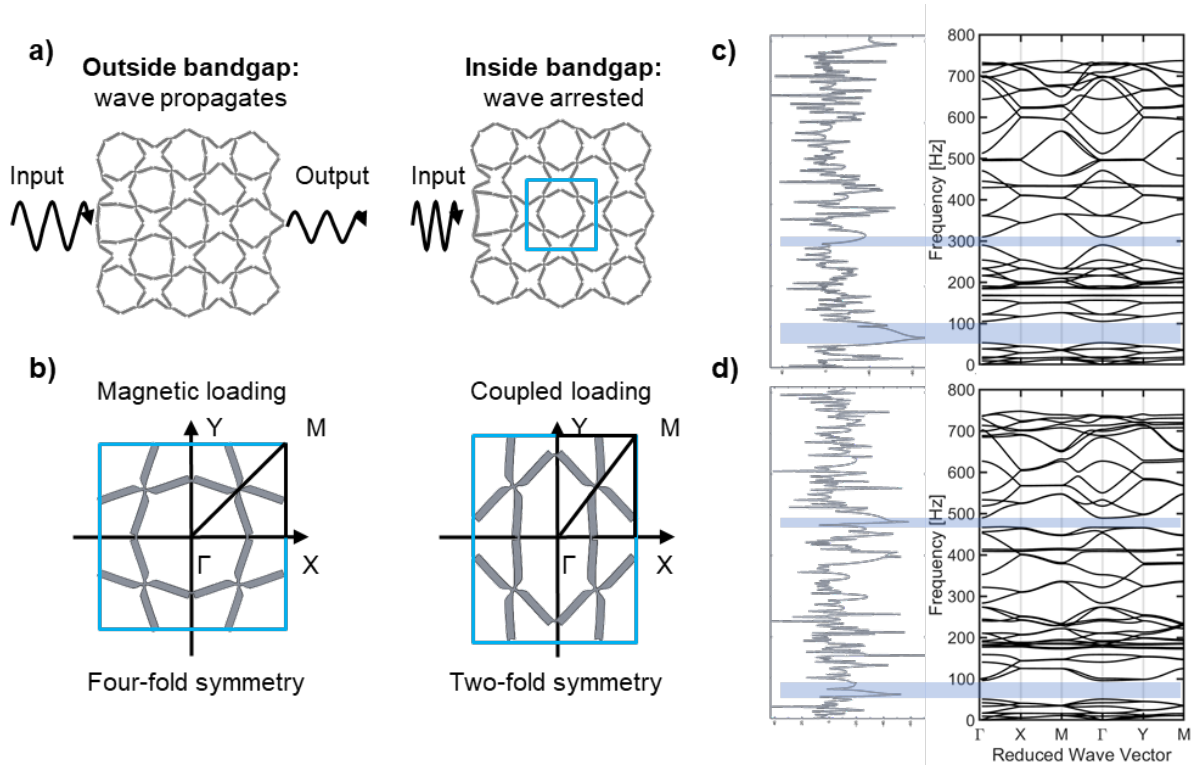

Figure S4. Summary of acoustic simulations. a) Demonstration of the inability for incident waves to propagate through the metamaterial if the frequency is within the bandgap. b) Outline of the IBZs for the magnetic loading (left) and coupled loading (right). c) Comparison of the dynamic simulation results to the Bloch method results at 15mT with no strain. d) Comparison of dynamics and Bloch results for the metamaterial under a 15mT field at 20% strain.

References:

1. Zhao R, Kim Y, Chester SA, Sharma P, Zhao X. Mechanics of hard-magnetic soft materials. J Mech Phys Solids. 2019;124:244-63.
2. Åberg M, Gudmundson P. The usage of standard finite element codes for computation of dispersion relations in materials with periodic microstructure. The Journal of the Acoustical Society of America. 1997;102(4):2007-13.
3. Kittel C. Elementary solid state physics: a short course: Wiley; 1962.
4. Brillouin L. Wave propagation in periodic structures: electric filters and crystal lattices: Courier Corporation; 2003.
5. Robillard J-F, Matar OB, Vasseur JO, Deymier PA, Stippinger M, Hladky-Hennion A-C, et al. Tunable magnetoelastic phononic crystals. Applied Physics Letters. 2009;95(12):124104.
6. Xu Z, Wu F, Guo Z. Shear-wave band gaps tuned in two-dimensional phononic crystals with magnetorheological material. Solid State Communications. 2013;154:43-5.